ACS APPLIED MATERIALS & INTERFACES

Research Article

Cite This: ACS Appl. Mater. Interfaces 2019, 11, 42349−42357

www.acsami.org

Joule-Heated and Suspended Silicon Nanowire Based Sensor for Low-Power and Stable Hydrogen Detection

Jeonghoon Yun,[†,‡] Jae-Hyuk Ahn,[∥] Dong-Il Moon,[§] Yang-Kyu Choi,[§] and Inkyu Park*[,†,‡]

[†]Department of Mechanical Engineering, [‡]KI for the NanoCentury, and [§]Department of Electrical Engineering, KAIST, Daejeon 305-701, Republic of Korea

[∥]Department of Electronic Engineering, Kwangwoon University, Seoul 01897, Republic of Korea

Supporting Information

ABSTRACT: We developed self-heated, suspended, and palladium-decorated silicon nanowires (Pd-SiNWs) for high-performance hydrogen (H_2) gas sensing with low power consumption and high stability against diverse environmental noises. To prepare the Pd-SiNWs, SiNWs were fabricated by conventional complementary metal−oxide−semiconductor (CMOS) processes, and Pd nanoparticles were coated on the SiNWs by a physical vapor deposition method. Suspended Pd-SiNWs were simply obtained by etching buried oxide layer and Pd deposition. Joule heating of Pd-SiNW (<1 mW) enables the detection of H_2 gas with a faster response and without the reduction of sensitivity unlike other Pd-based H_2 gas sensors. We proposed a H_2 sensing model using oxygen adsorption on the Pd nanoparticle-coated silicon oxide surface to understand the H_2 response of Joule-heated Pd-SiNWs. A suspended Pd-SiNW showed a similar transient sensing response with around four times lower Joule heating power (147 μW) than the substrate-bound Pd-SiNW (613 μW). The effect of interfering gas on the Pd-SiNW was investigated, and it was found that the Joule heating of Pd-SiNW helps to maintain the H_2 sensing performance in humid or carbon monoxide environments.

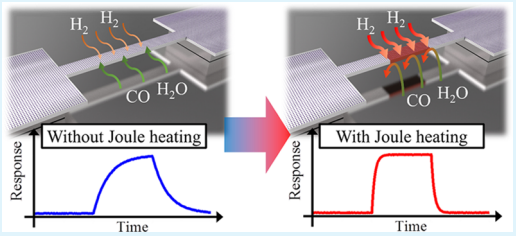

KEYWORDS: *hydrogen gas sensor, silicon nanowire, Joule heating, palladium, low-power sensor, isotherm*

1. INTRODUCTION

As the internet of things (IoT) market grows rapidly, the needs for low-cost and integrated sensors dramatically increased.[1−3] Among them, there have been many attempts to integrate gas sensors into the IoT devices toward personalized and distributed indoor/outdoor environmental monitoring.[4−7] These sensors measure gas concentrations by various methods such as electrochemical,[8] optical,[9] and chemiresistive mechanisms.[10−12] Among them, chemiresitive gas sensors have simple device structures and facile fabrication as compared with the other types and therefore provide a great advantage for realizing compact and integrated sensors.[11] For this reason, many studies have been conducted to develop microscale semiconductor-based chemiresistive gas sensors.[13−20] In general, semiconductor-based gas sensors are mainly composed of sensing materials (i.e., semiconductor materials) and heaters. Most semiconductor-based gas sensors require heaters because they exhibit good response characteristics with gases at high temperatures. Metal oxides typically have optimal operational temperatures of 200−400 °C, depending on the material composition. With the development of MEMS fabrication technology, microheaters have been integrated on microscale membranes, which could heat the sensor up to 300 °C with a driving power of 30 mW.[13,21] By improving the configuration from the membrane type to the bridge type, the power consumption for heating up to 300 °C could be reduced down to 1.5 mW.[17,22] However, the gas sensors operating with a few milliwatts still cannot be used for extended periods of time for portable electronic systems such as smartphones or nodes for the IoT applications.

As an alternative solution to this problem, nanoscale gas sensors with much lower power consumption have been introduced. In particular, gas sensors utilizing Joule heating of the sensing nanomaterial have been introduced to increase the operation temperature of the sensing material without the usage of an additional heater.[23−28] For example, Joule heating of tin oxide nanowires and carbon nanotubes was used for detecting nitrogen dioxide, reducing the power consumption from hundreds of microwatts to several microwatts.[23−26] However, previously developed self-heated nanomaterial-based devices have not been suitable for mass production because the fabrication process is neither repeatable nor high throughput due to the difficulty of integration of chemically synthesized nanomaterials on electronic devices. In this paper, we utilized a conventional top-down fabrication process of silicon nanowires (SiNWs) to develop self-heated and suspended palladium-coated silicon nanowires (Pd-SiNWs) and demonstrated Joule heating of SiNWs for fast hydrogen (H_2) detection as an example to confirm low power consumption and stable gas detection of a gas sensor based on self-heated SiNW. The self-heated SiNW is a generic approach that is not limited to H_2 gas detection only. It can be used for a variety of applications, but

Received: August 22, 2019
Accepted: October 16, 2019
Published: October 16, 2019

DOI: 10.1021/acsami.9b15111
ACS Appl. Mater. Interfaces 2019, 11, 42349−42357

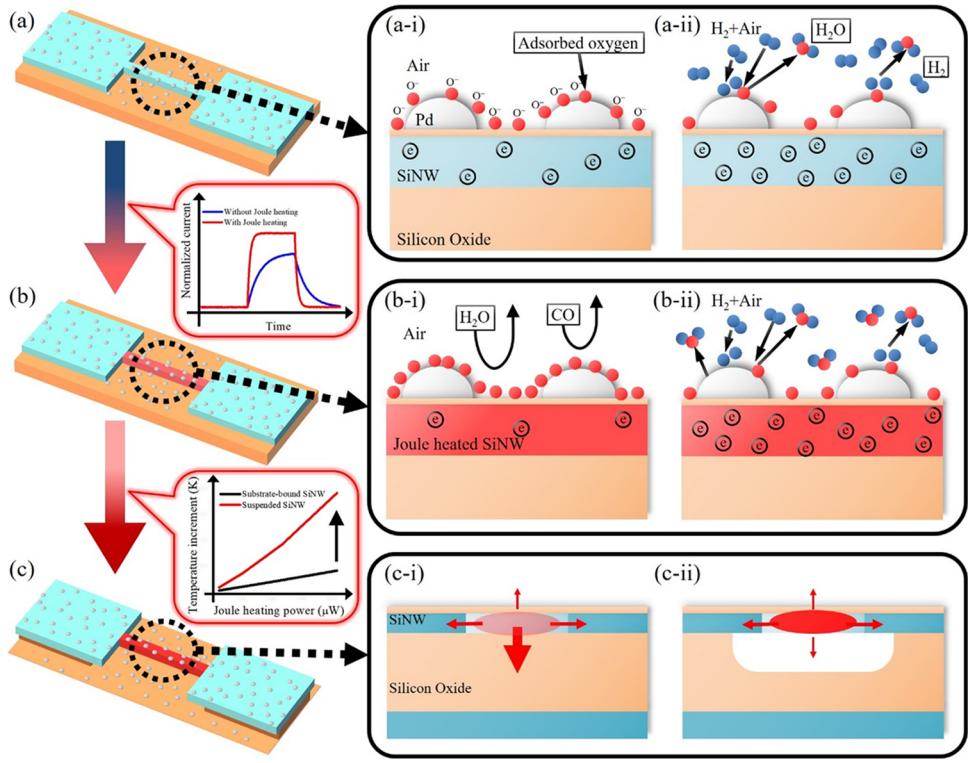

Figure 1. Working principle of H_2 sensing of a Pd-SiNW: (a) At room temperature, (a-i) depletion of charge carrier (electron) in SiNW (n-type) by negatively charged adsorbed oxygens (red dots) and (a-ii) accumulation of charge carrier by desorbing oxygen with H_2O formation under H_2 gas exposure; (b) Faster and higher response with Joule heating of Pd-SiNW because of (b-i) more depletion of charge carrier due to more adsorbed oxygen and (b-ii) fast reaction rate with H_2; Low interfering gas effect (H_2O and CO) with Joule heating; (c) Lowered power consumption by reducing heat loss through the substrate by changing from substrate-bound SiNW to suspended SiNW.

H_2 gas detection was used as an example in this study. This fabrication process enables cost-effective production of uniform Pd-SiNW gas sensors on waferscale. Since bare SiNWs respond to only a few gases such as ammonia and nitrogen dioxide, surface modification has been conducted to obtain the sensing characteristics for various gases.[29] Selective response to H_2 gas can be achieved by coating palladium (Pd) as a catalyst having a reactivity with H_2 gas. Pd is reactive to H_2 gas even at room temperature (Figure 1a), but its reaction is relatively slow and influenced by environmental factors such as humidity or carbon monoxide. By taking advantage of the self-heated (Figure 1b) and suspended structure (Figure 1c), Pd-SiNW could be Joule-heated at low power (submegawatt) to increase the reaction rate and reduce the degradation by humidity or carbon monoxide gas.

Pd-SiNW is not only suitable for mass production but also has several advantages compared to other self-Joule heating-based gas sensors. First, since metal oxide nanowires have high sensitivity, the temperature of the nanowire can vary much during detection because the resistance of a metal oxide nanowire can vary significantly and therefore the Joule heating power can be changed by a large amount.[24] To overcome this problem, a constant Joule heating power mode was used but the applied voltage had to be modulated in real-time, which may induce additional errors.[30] We demonstrated a moderately doped SiNW for Joule heating to reduce the power variation due to the large change in the electrical resistance. Although the sensitivity is lowered, it is comparable to the Pd-based H_2 gas sensors.[31,32] Second, according to the literature, the H_2 gas sensitivities of Pd nanowires are lowered when Joule heating is applied because of low H_2 solubility at high temperatures.[31,32] In contrast, we have found that the Joule heating of Pd-SiNW can accelerate the response to H_2 gas without sacrificing the sensitivity.

Figure 1 shows the working principle of a Pd-SiNW-based H_2 gas sensor with improved reaction rate and sensitivity by Joule heating. Negative surface charge builds up on Pd nanoparticles and silicon oxide (SiO_2) surface by adsorbing oxygen in the air environment.[33] When H_2 gas is exposed, adsorbed oxygen ions are desorbed by forming water (H_2O) molecules with H_2 and it causes the reduction of surface charge density on the surface of Pd-SiNW. Thus, the electrical conductivity of the Pd-SiNW is increased by the electron accumulation in the n-type Si (Figure 1a). Although the reactivity of Pd with H_2 exists at room temperature, both the response speed and sensitivity of the Pd-SiNW can be improved by increasing the temperature of Pd (Figure 1b). The response is faster at high temperatures because it is easier to overcome the activation energy. The sensitivity increases at high temperatures because it is dependent on the surface density of adsorbed oxygen, and the amount of spill-over oxygen is increased as the temperature is elevated.[34] Joule heating of the SiNW is an effective way to heat up Pd nanoparticles because it does not need an additional heater.[35] It can also minimize the effects of interfering molecules such as H_2O and CO that adsorb on the Pd surface and retard the surface reaction of H_2. The suspended structure of SiNW is more thermally efficient than the SiNW bounded on the SiO_2 layer (Figure 1c). Although the thermal conductivity of SiO_2 is low (1.4 $W{\cdot}m^{-1}{\cdot}K^{-1}$) at room temperature), the thermal conductivity of air (0.046 $W{\cdot}m^{-1}{\cdot}K^{-1}$ at room temperature) is

DOI: 10.1021/acsami.9b15111
ACS Appl. Mater. Interfaces 2019, 11, 42349−42357

much lower than that of SiO_2. By suspending the SiNW from the substrate, it is able to reduce heat loss to the substrate.

2. EXPERIMENTAL DETAIL

2.1. Pd-SiNW Fabrication. SiNWs were fabricated using conventional CMOS-compatible processes with silicon on an insulator (SOI, thickness of the top silicon layer = 40 nm; thickness of the buried oxide layer = 400 nm) wafer as a substrate. Deep ultraviolet lithography and oxygen plasma were used to define the photoresist pattern, and then it was transferred to the top Si layer by reactive ion etching (Figure 2a). To define the source and drain regions, the channel region was covered with photoresist and ion implantation (dopant = arsenic, energy = 25 keV, and dose = 5×10^{15} cm^{-2}) was performed. The fabricated SiNW had a width of 160 nm and a length of 500 nm. The SiNW channel region was doped by ion implantation (dopant = phosphorus, energy = 15 keV, and dose = 1×10^{14} cm^{-2}). Rapid thermal annealing was performed at 1000 °C for 10 s in a nitrogen atmosphere for the dopant activation. For gas sensors using SiNWs, lower doping concentration usually results in higher sensitivity. However, in this work, the electrical conductivity of SiNWs was intentionally increased to generate sufficient Joule heating by low bias voltages. Pd (1 nm-thick) was deposited on the SiNWs by electron beam evaporation. It is believed that the deposited Pd does not exist as a thin film but exist in the form of nanoparticles.[27,36] The suspended Pd-SiNWs were fabricated by removing the buried oxide layer before depositing Pd, as shown in Figure 2b.

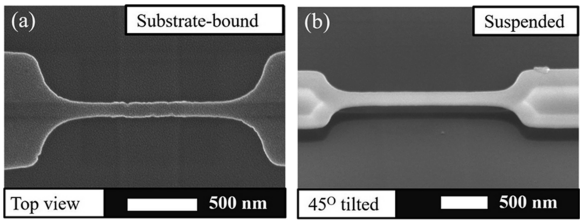

Figure 2. Scanning electron microscopy images of (a) substrate-bound and (b) suspended SiNWs.

2.2. Gas Sensing Test. Figure S1 shows a schematic image of the gas test setup. We used a synthetic air (79% nitrogen and 21% oxygen) as the base gas and measured the whole H_2 responses at room temperature without any external heating. The Pd-SiNW was heated by Joule heating of SiNW. The current change characteristics of Pd-SiNW were confirmed by changing the H_2 gas concentration from 0.01 to 0.5% and measured by a source meter (Keithley 2635B) with applying constant voltages. The response of Pd-SiNW is defined as $R = (I_{H_2} - I_{air})/I_{air} \times 100$ (%) in which I_{H_2} and I_{air} are the electrical currents in H_2 and air environments, respectively. The response time is defined as the time taken for the sensor signal to change from 20 to 80% of the total response ($\tau_{20-80\%}$), and the recovery time is defined as the time taken for the sensor signal to change from 80 to 20% of the total response ($\tau_{80-20\%}$). Humid air was adjusted by mixing dry air and wet air bubbled into a saturated potassium chloride solution in H_2O. Relative humidity was measured using a commercial relative humidity sensor (SHT3, Sensirion). Carbon monoxide (CO) was mixed with the gas mixture to confirm the effect of CO on the H_2 sensing performance of Pd-SiNW. The total flow rate of the mixture gas was kept constant at 500 sccm, and the volume of the chamber is approximately 60 cm^3. The flow rates and the source meter were controlled by the LabVIEW software.

3. RESULTS AND DISCUSSION

Figure 3 shows the H_2 gas sensing of the substrate-bound Pd-SiNW to the H_2 gas, while the Joule heating powers were controlled between 205 and 1172 μW (Figure 3a and see Figure S2 in the Supporting Information for raw data.). Each H_2 gas concentration was supplied for 100 s, and the measured electrical current of Pd-SiNW was normalized by the current in

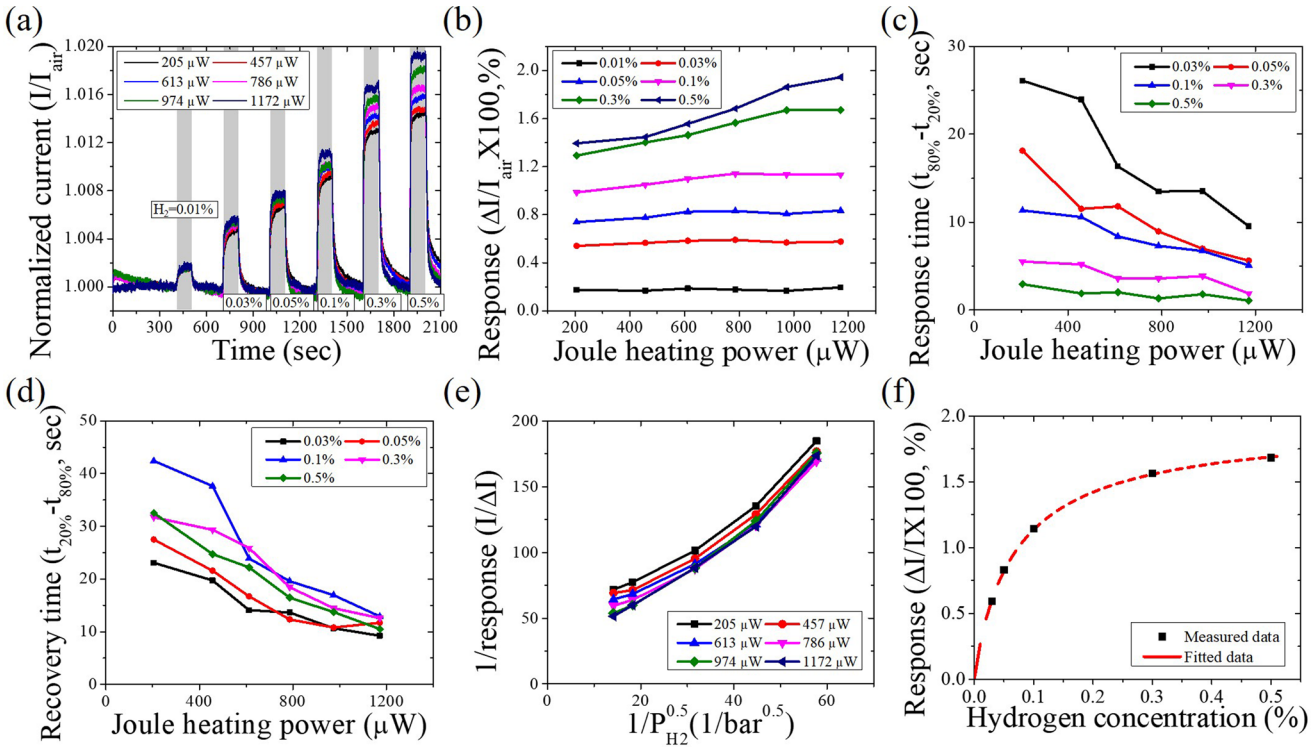

Figure 3. H_2 gas sensing of the substrate-bound Pd-SiNW sensor: (a) normalized current with Joule heating powers of 205, 457, 613, 786, 974, and 1172 μW; (b) response; (c) response time and (d) recovery time with respect to the Joule heating power; (e) linearized second-order Langmuir isotherm to H_2 pressure; and (f) response with a Joule heating power of 786 μW fitted by using the proposed model.

DOI: 10.1021/acsami.9b15111
ACS Appl. Mater. Interfaces 2019, 11, 42349−42357

the ambient air (base current). The electrical current of Pd-SiNW was increased by exposure to H_2 gas, and the higher current was observed as the H_2 gas concentration was increased. As explained above, it is believed that a 1 nm-thick Pd film does not directly affect the main electrical current of Pd-SiNW. The conductivity of Pd is decreased after converting to Pd hydride (PdH_x) upon exposure to H_2 gas,[37,38] but the current of Pd-SiNW is increased by the H_2 gas. It is presumed that the main electrical current passes through the SiNW rather than the Pd layer. Therefore, the sensing characteristics of Pd-SiNW are governed by the removal of adsorbed oxygen on Pd nanoparticles and SiO_2 surface under H_2 gas exposure. The estimated operating temperatures of Pd-SiNW were calculated by comparing the resistances of Pd-SiNW under external heating and self-Joule heating, and the estimated temperatures at Joule heating powers of 205 and 1172 μW were 67 and 225 °C, respectively (Figure S3). Figure 3b summarizes the response of Pd-SiNW to different H_2 gas concentrations under various Joule heating powers. The response of Pd-SiNW tends to increase with increasing Joule heating power of the Pd-SiNW. As mentioned in the previous paragraph, it is because the surface density of adsorbed oxygen on the Pd-SiNW is increased at high temperatures. Figure 3c,d shows the response time and recovery time of the Pd-SiNW sensor to different H_2 gas concentrations under various Joule heating powers. The response and recovery times are shortened by the higher Joule heating power, which causes faster rates of the H_2O forming reaction. Previously, Joule heating has been utilized in the Pd-based chemiresistive H_2 sensors (e.g., Pd nanowire sensors) to accelerate the speed of H_2 gas detection.[31,32] However, their responses to 0.5% $[H_2]$ were decreased by 23 times when a Joule heating power of 4.0 mW was applied because the solubility of H_2 is reduced at high temperatures.[31] On the other hand, the response of Pd-SiNW developed in this work was not deteriorated and even increased by the Joule heating. The response and recovery times of the Pd-SiNW are shorter than those of the Pd nanowire (PdNW)-based chemiresistive H_2 sensors. It has been reported that the response time of the PdNW-based chemiresistive H_2 sensor to 0.5% $[H_2]$ at room temperature was ~50 s in the literature.[31] On the contrary, the response time of the Pd-SiNW sensor is ~3 s to the same $[H_2]$ in this work. When Joule heating is given, the response time of the PdNW is ~2.5 s for the Joule heating power of 4.0 mW[31] while that of our Pd-SiNW was only 1.3 s for a Joule heating power of 786 μW. The response and recovery times of the Pd-SiNW are shorter than those of the PdNW because the Pd-SiNW utilizes surface reaction rather than interface reaction of hydrogen absorption into Pd. Even though the Pd-SiNW has relatively lower response than the metal oxide-based gas sensor, it can be overcome by using an electric circuit because of the high signalto-noise ratio (Figure S4). In addition, the lower response makes it able to reduce the disturbance of Joule heating power, which allows Joule heating with a constant voltage mode to be used instead of a constant power mode. We built a LabVIEW-based PID feedback control system to apply a constant Joule heating power of Pd-SiNW, and the results showed that the H_2 response with a constant voltage mode had a faster response than that with a constant power mode (Figure S5). We investigated the short-term stability of Joule-heated Pd-SiNW and the reproducibility of the same Pd-SiNW stored in an ambient environment for 2 weeks. The Joule-heated Pd-SiNW repeatably detected the H_2 gas, and the Joule heating of the Pd-SiNW was able to restore the H_2 gas sensing of contaminated Pd-SiNW (Figure S6). Hydrogen sulfide gas and ethanol vapor responses of Pd-SiNW were measured to investigate the selectivity of the Pd-SiNW sensor (Figure S7). We have verified that the H_2 selectivity of the proposed Pd-SiNW sensor is high enough for critical concentrations of various gases. H_2 detections using Joule heating of Pd or Pd-Si-based nanostructures are summarized in Table 1. Although the Joule heating power of Pd-SiNW is not the smallest among those of the nanostructures, Pd-SiNW has the fastest response time and shows a higher response ratio than the nanostructures. In summary, we found that the Joule heating of Pd-SiNW can shorten the response time with increasing the response.

Table 1. Comparison between Joule-Heated Nanostructure for H_2 Sensing

material	Joule heating power (mW)	response time[a] (s)	response ratio[b]	ref
Pd-SiNW	0.786	1.3 ($[H_2]$ = 0.5%)	1.21	this work
PdNW	4.0	2.5 ($[H_2]$ = 0.5%)	0.04	31
PdNW	0.13[c]	4.0 ($[H_2]$ = 2.4%)	0.36	31 and 32
Pt-Si nanobelt	2.4[c]	2.6 ($[H_2]$ = 0.1%)	0.39	39
Pd-network	500[c]	13 ($[H_2]$ = 1%)	0.46	40

[a]Response time at stated $[H_2]$. [b]Response ratio (= response with Joule heating/response without Joule heating). [c]Calculated value.

There were several studies to describe H_2 adsorption isotherms on the bilayer of palladium-silicon.[41−43] A physical model of electric dipole induced by hydrogen atoms at the interface between Pd and SiO_2 layers was developed to describe the threshold voltage shift of a Pd-gate FET.[44,45] The second-order Langmuir isotherm and logarithmic model were used for representing the threshold voltage shift of a Pd-gate FET under H_2 exposure.[41,42] The previous papers utilized a thick and continuous Pd film as a gas-sensitive layer. However, our H_2 gas sensor of Pd-SiNW utilizes a nanoparticle-like discontinuous Pd film. Thus, we believe that the H_2 response of Pd-SiNW is not fitted with the second-order Langmuir isotherm. In the second-order Langmuir isotherm, the reciprocal of coverage is proportional to the reciprocal of square root of partial gas pressure of the adsorbate. As shown in Figure 3e, our measured data does not have linearity between the reciprocal of response and the reciprocal of square root of H_2 gas pressure. We adopted an oxygen adsorption model with H_2 gas to represent the H_2 isotherm of Pd-SiNW. The coverage of adsorbed oxygen is derived by $\theta = \theta_0(1 - l)$, where θ_0 is the coverage of adsorbed oxygen without H_2 gas and l is ratio of decrement of adsorbed oxygen by H_2 gas. Adsorption kinetics of oxygen is derived by $d\theta/dt = k_1 P_{O_2}[1 - \theta_0(1 - l)]^2$, where k_1 is the adsorption kinetic constant and P_{O_2} is the partial pressure of oxygen gas. Desorption kinetics of oxygen is derived by $d\theta/dt = k_2[\theta_0(1 - l)]^2 + k_3 P_{H_2}[\theta_0(1 - l)]$, where k_2 is the desorption kinetic constant, k_3 is the H_2O forming reaction constant, and P_{H_2} is the partial pressure of H_2 gas. In the equilibrium state, l is

DOI: 10.1021/acsami.9b15111
ACS Appl. Mater. Interfaces 2019, 11, 42349−42357

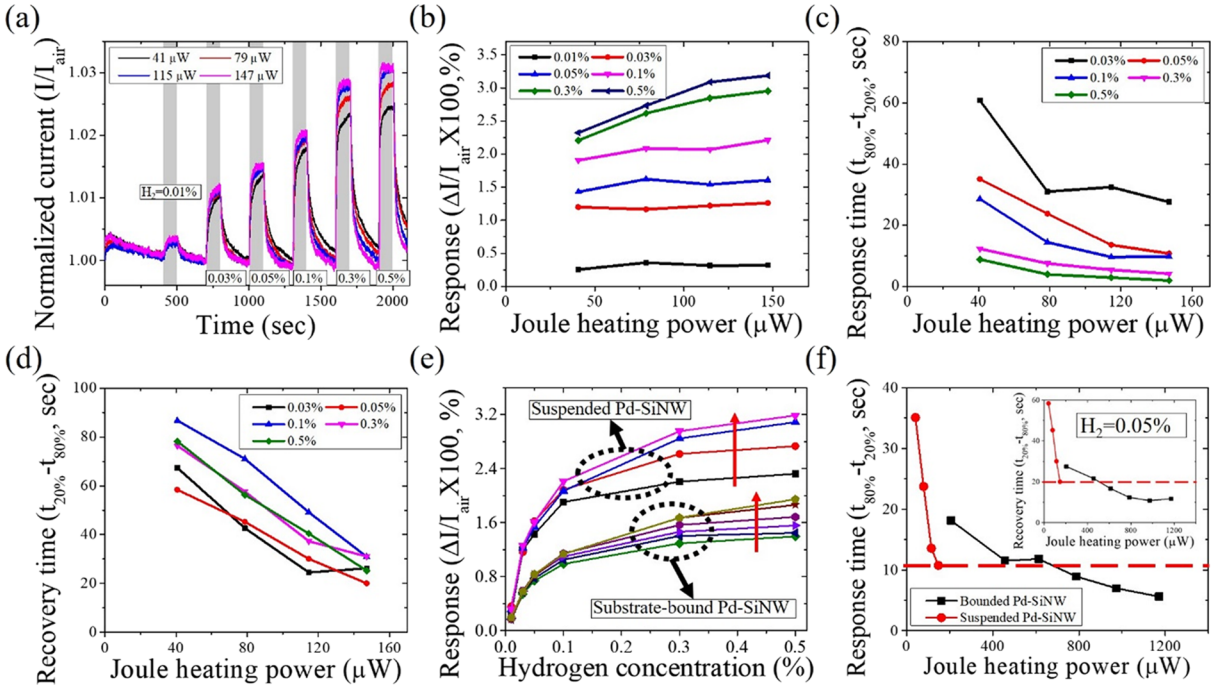

Figure 4. H_2 gas sensing of the suspended Pd-SiNW sensor: (a) normalized current with Joule heating powers of 41, 79, 115, and 147 μW; (b) response; (c) response time; (d) recovery time with respect to the Joule heating power. Comparison between the substrate-bound and suspended Pd-SiNW sensors: (e) responses with various Joule heating powers (red arrows: direction of Joule heating power increment (from 41 to 147 μW for the suspended Pd-SiNW and from 205 to 1172 μW for the substrate-bound Pd-SiNW)) and (f) response time and (inset in (f)) recovery time for 0.05% [H_2] (red dotted line indicates the similarity of transient behavior between the suspended Pd-SiNW at a Joule heating power of 147 and the substrate-bound Pd-SiNW at a Joule heating power of 613 μW).

$$\left(-\left[\frac{k_2}{k_3}\theta_0\left(\frac{\theta_0}{1-\theta_0}+1\right)+\frac{P_{H_2}}{2}\right]+\sqrt{\left(\frac{k_2}{k_3}\theta_0\left(\frac{\theta_0}{1-\theta_0}+1\right)+\frac{P_{H_2}}{2}\right)^2+\frac{k_2}{k_3}\theta_0\left(\left(\frac{\theta_0}{1-\theta_0}\right)^2-1\right)P_{H_2}}\right)\Bigg/\left(\frac{k_2}{k_3}\theta_0\left(\left(\frac{\theta_0}{1-\theta_0}\right)^2-1\right)\right)$$

Since response (R) is proportional to the surface charge change

$$R \propto \Delta\theta = (\theta_0 - \theta_0(1-l)) = \theta_0 l$$

The measured response is fitted by using the least square method, and Figure 3f shows the measured and fitted responses with a Joule heating power of 786 μW. The fitted response is in good agreement with the measured response (see Supporting Information for detailed description). Because θ_0 is increased by elevating the temperature, response is increased by applying a higher Joule heating power.

Figure 4a presents the H_2 gas sensing of the suspended Pd-SiNW sensor to the H_2 gas with concentrations from 0.01 to 0.5%, while the Joule heating powers were varied from 41 to 147 μW. Similar to the substrate-bound Pd-SiNW sensor, the sensing rate of the suspended Pd-SiNW sensor was improved by the Joule heating without sacrificing the response (Figure 4b–d). In addition, it was observed that the suspended Pd-SiNW sensor has a higher response (Figure 4e) and lower conductivity than the substrate-bound Pd-SiNW sensor. The fixed oxide charge is a positive charge located at the interface between the top Si layer and the buried SiO_2 layer, which induces an effective positive gate voltage on the SiNW.[46] After etching the buried SiO_2 layer, the fixed oxide charge is eliminated and simultaneously oxygen is adsorbed. The effective gate potential induced by eliminating the fixed oxide charge and adsorbing oxygen is negatively shifted, and this lowers the conductivity of the n-type Si. In our previous study, we verified the gate effect of the Pd-SiNW sensor and observed that the Pd-coated SiNW field effect transistor shows the highest sensitivity at the subthreshold regime and that the negative shift of gate voltage above the threshold regime increases the response of the n-type SiNW.[47] Meanwhile, the bottom side of suspended Pd-SiNW does not contribute to enhancing the H_2 response because bare SiNW without Pd coating does not have a H_2 response (Figure S9). Nevertheless, the suspended Pd-SiNW has a higher response than the substrate-bound Pd-SiNW due to the negative shift of effective gate voltage of SiNW. Assuming that the response time is solely dependent on the temperature, it can be said that the two structures (i.e., substrate-bound and suspended Pd-SiNWs) with the same response time are at the same temperature.[48] As shown in Figure 4f, the suspended Pd-SiNW at a Joule heating power of 147 μW performs similar transient response as the substrate-bound Pd-SiNW at a Joule heating power of 613 μW. This result proves a dramatic reduction of power required to induce the Joule heating of the Pd-SiNW (by ~4.17 times for the same temperature). In the substrate-bound SiNWs, the heat generated by the Joule heating of the SiNW is dissipated into the substrate (Figures S10 and S11). Suspending the SiNW from the substrate results in a higher temperature than the substrate-bound SiNW under the same Joule heating power. This is due to the much smaller thermal conductivity of air (0.06 $W \cdot m^{-1} \cdot K^{-1}$) than that of SiO_2

DOI: 10.1021/acsami.9b15111
ACS Appl. Mater. Interfaces 2019, 11, 42349–42357

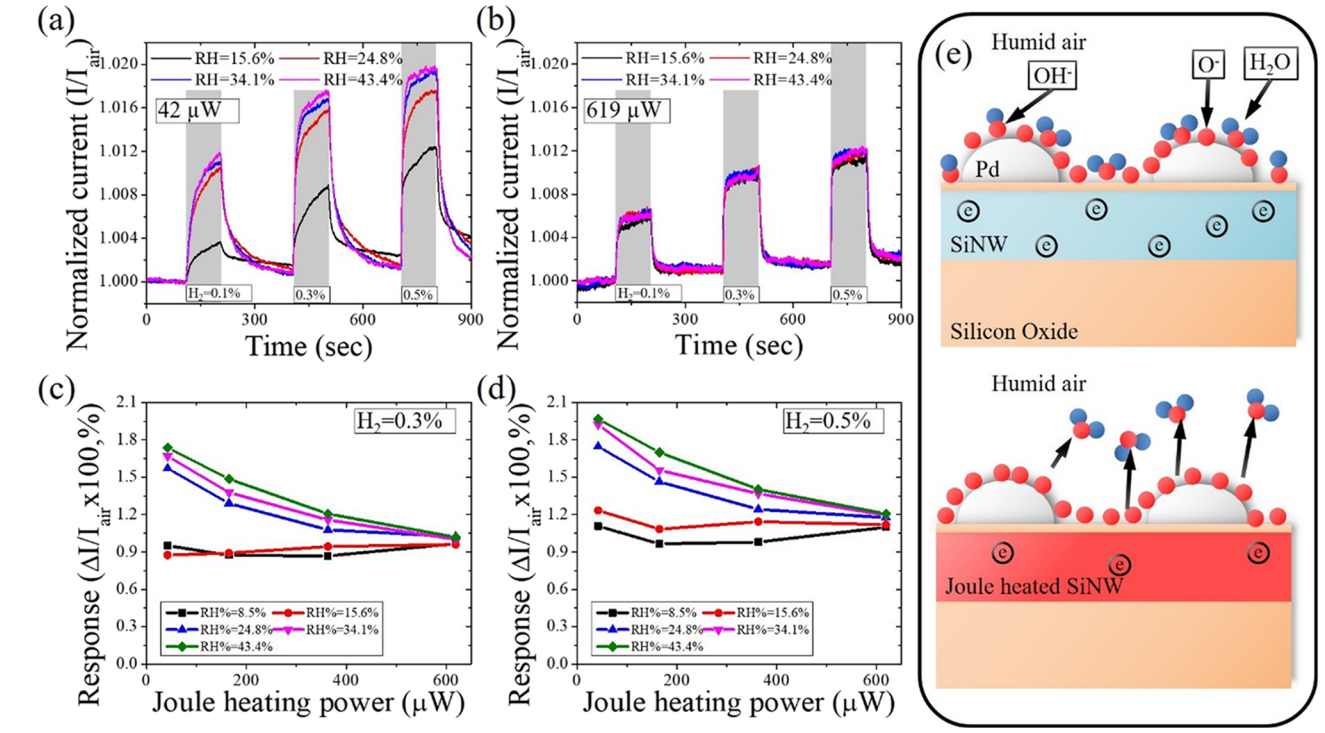

Figure 5. Humidity effect of Pd-SiNW for H_2 gas sensing: normalized current with different relative humidities at (a) low (42 μW) and (b) high (619 μW) Joule heating powers; (c, d) responses according to different Joule heating powers; (e) adsorbed H_2O and hydroxyl species on Pd-SiNW under humid air at room temperature and with Joule heating of Pd-SiNW.

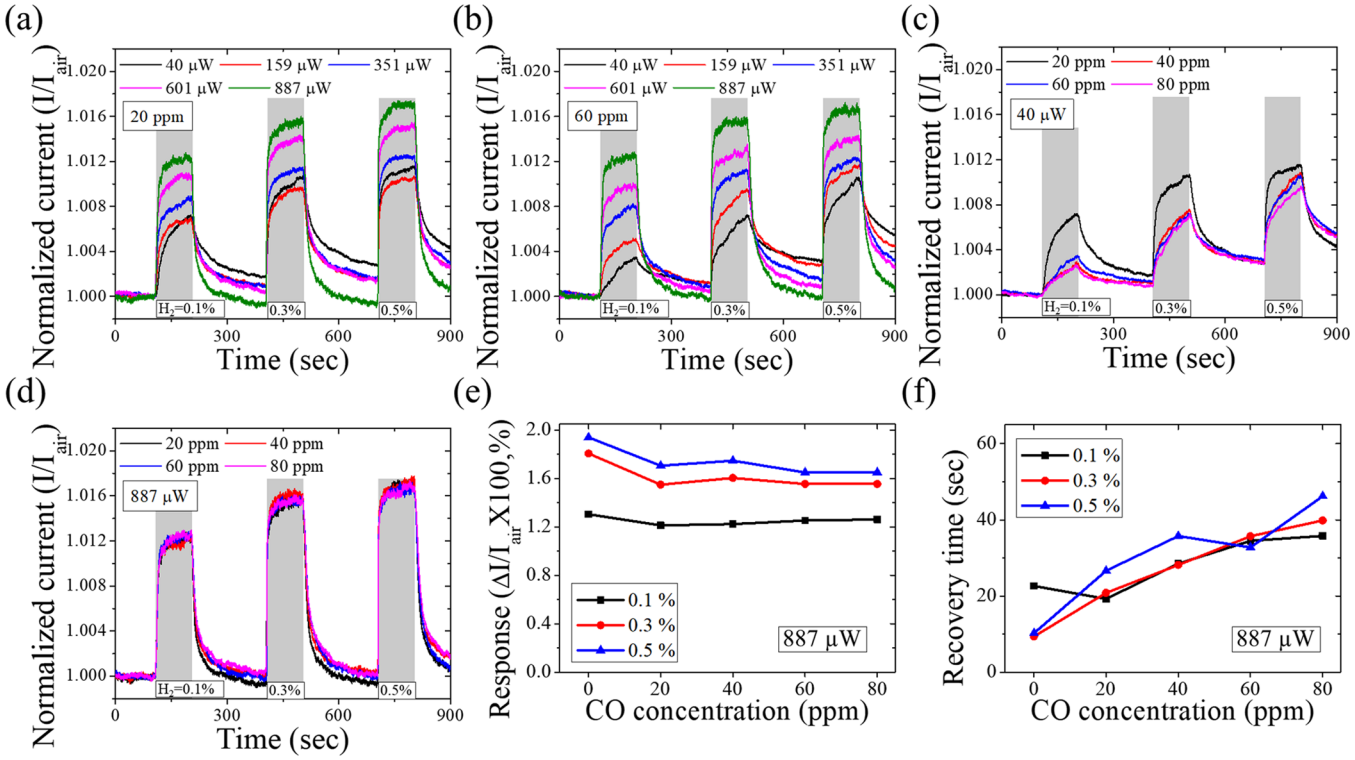

Figure 6. Carbon monoxide (CO) effect of Pd-SiNW for H_2 gas sensing: normalized current at (a) 20 ppm of CO and (b) 60 ppm of CO; normalized current under Joule heating powers of (c) 40 μW and (d) 887 μW; and (e) response and (f) recovery time at a Joule heating power of 887 μW with respect to various CO concentrations.

(1.4 $W \cdot m^{-1} \cdot K^{-1}$), which dramatically reduces the conductive heat dissipation from the Joule-heated SiNW to the substrate. Numerical calculation shows that the temperature increment of suspended SiNW (144 K) is about 3.7 times higher than that of substrate-bound SiNW (39 K) with a Joule heating of 200 μW. Thus, the suspended SiNW can reduce power

DOI: 10.1021/acsami.9b15111
ACS Appl. Mater. Interfaces 2019, 11, 42349−42357

consumption by around 75% compared with the substrate-bound SiNW.

When the H_2 gas sensor is used in real-life applications, various interfering gases can be present in the atmosphere. Among them, H_2O molecules exist everywhere with continuously varying concentrations (i.e., relative humidity). As the H_2O molecules attach to the surface of Pd-SiNW, the reactivity between H_2 gas and adsorbed oxygen could be reduced by the hindrance of H_2O molecules.[49] Another interfering gas is CO, which is generated in a steam reforming-based H_2 production process. When CO is adsorbed on the Pd surface, the activation energy required to adsorb H_2 to the Pd surface increases.[50] Therefore, the Pd-based H_2 sensor exhibits a slow reaction rate to H_2 gas with the presence of CO. The influence of the interference factors was confirmed by controlling the relative humidity and by mixing with CO gas in the H_2 gas detection of Pd-SiNW. As shown in Figure 5a,b, when the Pd-SiNW with a low Joule heating power is exposed to higher humidity, the reaction rate to H_2 gas is lowered and the response changed. However, as the Joule heating power is increased, faster reaction rate and lower humidity dependency of response are observed. When H_2O molecules are exposed to the surface, not only the H_2O molecules adhere to the surface but also hydroxyl species are formed. Physisorbed H_2O molecules slow down the reaction between H_2 and adsorbed oxygen, and negatively charged hydroxyl species cause a response change similar to that discussed for the effective gate voltage. At elevated temperatures, H_2O molecules and hydroxyl species are removed from the Pd surface, as shown in Figure 5e.[51] Figure 5c,d presents the responses of Pd-SiNW sensor to 0.3 and 0.5% [H_2] at different Joule heating powers. The response of Pd-SiNW increases with the relative humidity at a low Joule heating power (42 μW, estimated temperature = 33 °C) because of the hydroxyl species. However, the response is not significantly affected by the relative humidity when a Joule heating power of 620 μW (estimated temperature = 130 °C) is applied. Therefore, the Joule heating of the Pd-SiNW is able to restore the H_2 gas sensing of the Pd-SiNW from various humidity conditions.

Figure 6 shows the effect of CO on the H_2 gas sensing. When CO gas was mixed into H_2 gases, the response rate of the Pd-SiNW sensor was significantly lowered and the current was not saturated within 100 s at a low Joule heating power (40 μW, Figure 6c). In addition, slow recovery of Pd-SiNW was observed, and the signal was not fully returned to the initial value. At a high Joule heating power (887 μW, Figure 6d–f), the response was maintained at similar values regardless of CO concentrations and the response rate was fast enough to observe the saturation of signal. The slow rates were still observed even when a high Joule heating power was applied, and the slower rate was measured as increasing the concentration of CO (Figure 6f). It is believed that when more CO molecules are adsorbed on Pd nanoparticles, they increase the activation energy of H_2 adsorption on Pd. In summary, we confirmed that the Joule heating of Pd-SiNW can reduce the influence of CO gas when detecting H_2 gas.

4. CONCLUSIONS

We developed a H_2 gas sensor using Pd-SiNW and a low-power H_2 sensing technology that enable rapid detection without response degradation using the Joule heating of Pd-SiNW. We fabricated a H_2 sensor operating at sub-milliwatt power by the formation of suspended Pd-SiNW and confirmed that the H_2 detection characteristics are comparable to those of the substrate-bound Pd-SiNW at much lower operation power. The oxygen adsorption model for H_2 response of Pd-SiNW was adopted to understand the results of increased response with Joule heating of Pd-SiNW. In addition, the Joule heating of Pd-SiNW was found to reduce the influence of humidity and CO on the sensing characteristics to H_2 gas. Since Pd-SiNW can be easily fabricated by conventional CMOS nano-fabrication processes, mass production is possible with easy integration of electric circuit elements and high uniformity and reproducibility of sensors can be realized. It is expected that the self-heated, suspended Pd-SiNW sensors will provide an alternative to the existing chemiresistive H_2 sensors with their advantages such as low electrical power consumption, fast response, and improved stability against CO and humidity.

■ ASSOCIATED CONTENT

Supporting Information

The Supporting Information is available free of charge on the ACS Publications website at DOI: 10.1021/acsami.9b15111.

Gas test setup; raw data of Figure 3a in the main text; temperature estimation of the Joule-heated silicon nanowire; signal-to-noise ratio of Pd-SiNW; constant Joule heating mode; reproducibility of Joule-heated Pd-SiNW; selectivity of the Joule-heated Pd-SiNW sensor; oxygen adsorption isotherm with hydrogen gas; hydrogen response of bare silicon nanowire; and numerical calculation of Joule-heated silicon nanowire (PDF)

■ AUTHOR INFORMATION

Corresponding Author

*E-mail: inkyu@kaist.ac.kr.

ORCID

Jae-Hyuk Ahn: 0000-0001-7490-000X
Yang-Kyu Choi: 0000-0001-6678-5451
Inkyu Park: 0000-0001-5761-7739

Notes

The authors declare no competing financial interest.

■ ACKNOWLEDGMENTS

This research was supported by Nano Material Technology Development Program (2015M3A7B7045518) through the National Research Foundation of Korea (NRF) funded by the Ministry of Science, ICT & Future Planning, (MSIP). This research was also supported by Multi-Ministry Collaborative R&D Program (Development of Techniques for Identification and Analysis of Gas Molecules to Protect Against Toxic Substances) through the National Research Foundation of Korea (NRF -2017M3D9A1073858). This research was also supported by the KUSTAR-KAIST Institute, KAIST, Korea.

■ REFERENCES

(1) Stankovic, J. A. Research Directions for the Internet of Things. *IEEE Internet of Things Journal;* IEEE: 2014, *1*, 3–9.
(2) Zanella, A.; Bui, N.; Castellani, A.; Vangelista, L.; Zorzi, M. Internet of Things for Smart Cities. *IEEE Internet of Things Journal;* IEEE: 2014, *1*, 22–32.
(3) Gubbi, J.; Buyya, R.; Marusic, S.; Palaniswami, M. Internet of Things (Iot): A Vision, Architectural Elements, and Future Directions. *Future. Gener. Comput. Syst.* **2013**, *29*, 1645–1660.
(4) Kampa, M.; Castanas, E. Human Health Effects of Air Pollution. *Environ. Pollut.* **2008**, *151*, 362–367.

DOI: 10.1021/acsami.9b15111
ACS Appl. Mater. Interfaces 2019, 11, 42349–42357

(5) Franklin, P. J. Indoor Air Quality and Respiratory Health of Children. *Paediatr. Respir. Rev.* **2007**, *8*, 281−286.
(6) Bernstein, J. A.; Alexis, N.; Bacchus, H.; Bernstein, I. L.; Fritz, P.; Horner, E.; Li, N.; Mason, S.; Nel, A.; Oullette, J.; Reijula, K.; Reponen, T.; Seltzer, J.; Smith, A.; Tarlo, S. M. The Health Effects of Non-Industrial Indoor Air Pollution. *J. Allergy Clin. Immunol.* **2008**, *121*, 585−591.
(7) Suh, J.-H.; Cho, I.; Kang, K.; Kweon, S.-J.; Lee, M.; Yoo, H.-J.; Park, I. Fully Integrated and Portable Semiconductor-Type Multi-Gas Sensing Module for Iot Applications. *Sens. Actuators, B* **2018**, *265*, 660−667.
(8) Korotcenkov, G.; Han, S. D.; Stetter, J. R. Review of Electrochemical Hydrogen Sensors. *Chem. Rev.* **2009**, *109*, 1402−1433.
(9) Hodgkinson, J.; Tatam, R. P. Optical Gas Sensing: A Review. *Meas. Sci. Technol.* **2013**, *24*, No. 012004.
(10) Sun, Y.-F.; Liu, S.-B.; Meng, F.-L.; Liu, J.-Y.; Jin, Z.; Kong, L.-T.; Liu, J.-H. Metal Oxide Nanostructures and Their Gas Sensing Properties: A Review. *Sensors* **2012**, *12*, 2610−2631.
(11) Fine, G. F.; Cavanagh, L. M.; Afonja, A.; Binions, R. Metal Oxide Semi-Conductor Gas Sensors in Environmental Monitoring. *Sensors* **2010**, *10*, 5469−5502.
(12) Yang, D.; Fuadi, M. K.; Kang, K.; Kim, D.; Li, Z.; Park, I. Multiplexed Gas Sensor Based on Heterogeneous Metal Oxide Nanomaterial Array Enabled by Localized Liquid-Phase Reaction. *ACS Appl. Mater. Interfaces* **2015**, *7*, 10152−10161.
(13) Baroncini, M.; Placidi, P.; Cardinali, G. C.; Scorzoni, A. Thermal Characterization of a Microheater for Micromachined Gas Sensors. *Sens. Actuators, A* **2004**, *115*, 8−14.
(14) Spannhake, J.; Schulz, O.; Helwig, A.; Krenkow, A.; Müller, G.; Doll, T. High-Temperature Mems Heater Platforms: Long-Term Performance of Metal and Semiconductor Heater Materials. *Sensors* **2006**, *6*, 405−419.
(15) Lee, K.-N.; Lee, D.-S.; Jung, S.-W.; Jang, Y.-H.; Kim, Y.-K.; Seong, W.-K. A High-Temperature Mems Heater Using Suspended Silicon Structures. *J. Micromech. Microeng.* **2009**, *19*, 115011.
(16) Hwang, W.-J.; Shin, K.-S.; Roh, J.-H.; Lee, D.-S.; Choa, S.-H. Development of Micro-Heaters with Optimized Temperature Compensation Design for Gas Sensors. *Sensors* **2011**, *11*, 2580−2591.
(17) Zhou, Q.; Sussman, A.; Chang, J.; Dong, J.; Zettl, A.; Mickelson, W. Fast Response Integrated Mems Microheaters for Ultra Low Power Gas Detection. *Sens. Actuators, A* **2015**, *223*, 67−75.
(18) Kang, K.; Yang, D.; Park, J.; Kim, S.; Cho, I.; Yang, H.-H.; Cho, M.; Mousavi, S.; Choi, K. H.; Park, I. Micropatterning of Metal Oxide Nanofibers by Electrohydrodynamic (Ehd) Printing Towards Highly Integrated and Multiplexed Gas Sensor Applications. *Sens. Actuators, B* **2017**, *250*, 574−583.
(19) Kim, D.; Yang, D.; Kang, K.; Lim, M. A.; Li, Z.; Park, C.-O.; Park, I. In-Situ Integration and Surface Modification of Functional Nanomaterials by Localized Hydrothermal Reaction for Integrated and High Performance Chemical Sensors. *Sens. Actuators, B* **2016**, *226*, 579−588.
(20) Yang, D.; Kim, D.; Ko, S. H.; Pisano, A. P.; Li, Z.; Park, I. Focused Energy Field Method for the Localized Synthesis and Direct Integration of 1d Nanomaterials on Microelectronic Devices. *Adv. Mater.* **2015**, *27*, 1207−1215.
(21) Afridi, M. Y.; Suehle, J. S.; Zaghloul, M. E.; Berning, D. W.; Hefner, A. R.; Cavicchi, R. E.; Semancik, S.; Montgomery, C. B.; Taylor, C. J. A Monolithic Cmos Microhotplate-Based Gas Sensor System. *IEEE Sens. J.* **2002**, *2*, 644−655.
(22) Cho, I.; Kang, K.; Yang, D.; Yun, J.; Park, I. Localized Liquid-Phase Synthesis of Porous Sno_2 Nanotubes on Mems Platform for Low-Power, High Performance Gas Sensors. *ACS Appl. Mater. Interfaces* **2017**, *9*, 27111−27119.
(23) Prades, J. D.; Jimenez-Diaz, R.; Hernandez-Ramirez, F.; Cirera, A.; Romano-Rodriguez, A.; Morante, J. R. Harnessing Self-Heating in Nanowires for Energy Efficient, Fully Autonomous and Ultra-Fast Gas Sensors. *Sens. Actuators, B* **2010**, *144*, 1−5.
(24) Meng, G.; Zhuge, F.; Nagashima, K.; Nakao, A.; Kanai, M.; He, Y.; Boudot, M.; Takahashi, T.; Uchida, K.; Yanagida, T. Nanoscale Thermal Management of Single Sno2nanowire: Pico-Joule Energy Consumed Molecule Sensor. *ACS Sensors* **2016**, *1*, 997−1002.
(25) Strelcov, E.; Dmitriev, S.; Button, B.; Cothren, J.; Sysoev, V.; Kolmakov, A. Evidence of the Self-Heating Effect on Surface Reactivity and Gas Sensing of Metal Oxide Nanowire Chemiresistors. *Nanotechnology* **2008**, *19*, 355502.
(26) Zhang, J.; Strelcov, E.; Kolmakov, A. Heat Dissipation from Suspended Self-Heated Nanowires: Gas Sensor Prospective. *Nanotechnology* **2013**, *24*, 444009.
(27) Ahn, J.-H.; Yun, J.; Moon, D.-I.; Choi, Y.-K.; Park, I. Self-Heated Silicon Nanowires for High Performance Hydrogen Gas Detection. *Nanotechnology* **2015**, *26*, No. 095501.
(28) Yun, J.; Jin, C. Y.; Ahn, J. H.; Jeon, S.; Park, I. A Self-Heated Silicon Nanowire Array: Selective Surface Modification with Catalytic Nanoparticles by Nanoscale Joule Heating and Its Gas Sensing Applications. *Nanoscale* **2013**, *5*, 6851−6856.
(29) Cao, A.; Sudhölter, E. J.; de Smet, L. C. P. M. Silicon Nanowire-Based Devices for Gas-Phase Sensing. *Sensors* **2014**, *14*, 245−271.
(30) Tan, H. M.; Manh Hung, C.; Ngoc, T. M.; Nguyen, H.; Duc Hoa, N.; Van Duy, N.; Hieu, N. V. Novel Self-Heated Gas Sensors Using on-Chip Networked Nanowires with Ultralow Power Consumption. *ACS Appl. Mater. Interfaces* **2017**, *9*, 6153−6162.
(31) Yang, F.; Taggart, D. K.; Penner, R. M. Joule Heating a Palladium Nanowire Sensor for Accelerated Response and Recovery to Hydrogen Gas. *Small* **2010**, *6*, 1422−1429.
(32) Offermans, P.; Tong, H. D.; van Rijn, C. J. M.; Merken, P.; Brongersma, S. H.; Crego-Calama, M. Ultralow-Power Hydrogen Sensing with Single Palladium Nanowires. *Appl. Phys. Lett.* **2009**, *94*, 223110.
(33) Gupta, D.; Dutta, D.; Kumar, M.; Barman, P. B.; Sarkar, C. K.; Basu, S.; Hazra, S. K. A Low Temperature Hydrogen Sensor Based on Palladium Nanoparticles. *Sens. Actuators, B* **2014**, *196*, 215−222.
(34) Eriksson, M.; Petersson, L. G. Spillover of Hydrogen, Oxygen and Carbon-Monoxide in Oxidation Reactions on Sio_2 Supported Pd. *Surf. Sci.* **1994**, *311*, 139−152.
(35) Yun, J.; Ahn, J.-H.; Lee, B. J.; Moon, D.-I.; Choi, Y.-K.; Park, I. Temperature Measurement of Joule Heated Silicon Micro/Nanowires Using Selectively Decorated Quantum Dots. *Nanotechnology* **2016**, *27*, 505705.
(36) Nah, J.; Kumar, S. B.; Fang, H.; Chen, Y.-Z.; Plis, E.; Chueh, Y.-L.; Krishna, S.; Guo, J.; Javey, A. Quantum Size Effects on the Chemical Sensing Performance of Two-Dimensional Semiconductors. *J. Phys. Chem. C* **2012**, *116*, 9750−9754.
(37) Hughes, R. C.; Schubert, W. K. Thin Films of Pd/Ni Alloys for Detection of High Hydrogen Concentrations. *J. Appl. Phys.* **1992**, *71*, 542−544.
(38) Cho, M.; Zhu, J.; Kim, H.; Kang, K.; Park, I. Half-Pipe Palladium Nanotube-Based Hydrogen Sensor Using a Suspended Nanofiber Scaffold. *ACS Appl. Mater. Interfaces* **2019**, *11*, 13343−13349.
(39) Tran, N. A.; Pan, F.-M.; Sheu, J.-T. Hydrogen Gas Sensors from Polysilicon Nanobelt Devices Selectively Modified with Sensing Materials. *Nanotechnology* **2016**, *27*, 505604.
(40) Walia, S.; Gupta, R.; Rao, K. D. M.; Kulkarni, G. U. Transparent Pd Wire Network-Based Areal Hydrogen Sensor with Inherent Joule Heater. *ACS Appl. Mater. Interfaces* **2016**, *8*, 23419−23424.
(41) Robins, I.; Ross, J. F.; Shaw, J. E. A. The Logarithmic Response of Palladium-Gate Metal-Insulator-Silicon Field-Effect Transistors to Hydrogen. *J. Appl. Phys.* **1986**, *60*, 843−845.
(42) Morita, Y.; Nakamura, K.; Kim, C. Langmuir Analysis on Hydrogen Gas Response of Palladium-Gate Fet. *Sens. Actuators, B* **1996**, *33*, 96−99.
(43) Ekedahl, L.-G.; Eriksson, M.; Lundström, I. Hydrogen Sensing Mechanisms of Metal−Insulator Interfaces. *Acc. Chem. Res.* **1998**, *31*, 249−256.

DOI: 10.1021/acsami.9b15111
ACS Appl. Mater. Interfaces 2019, 11, 42349−42357

(44) Lundström, I.; Distefano, T. Hydrogen Induced Interfacial Polarization at Pd-Sio2 Interfaces. *Surf. Sci.* **1976**, *59*, 23−32.
(45) Lundström, I. Hydrogen Sensitive Mos-Structures. *Sens. Actuators* **1981**, *1*, 403−426.
(46) Deal, B. E.; Sklar, M.; Grove, A. S.; Snow, E. H. Characteristics of the Surface-State Charge (Q_{ss}) of Thermally Oxidized Silicon. *J. Electrochem. Soc.* **1967**, *114*, 266−274.
(47) Ahn, J.-H.; Yun, J.; Choi, Y.-K.; Park, I. Palladium Nanoparticle Decorated Silicon Nanowire Field-Effect Transistor with Side-Gates for Hydrogen Gas Detection. *Appl. Phys. Lett.* **2014**, *104*, No. 013508.
(48) Prades, J. D.; Jimenez-Diaz, R.; Hernandez-Ramirez, F.; Barth, S.; Cirera, A.; Romano-Rodriguez, A.; Mathur, S.; Morante, J. R. Ultralow Power Consumption Gas Sensors Based on Self-Heated Individual Nanowires. *Appl. Phys. Lett.* **2008**, *93*, 123110.
(49) Baselt, D. R.; Fruhberger, B.; Klaassen, E.; Cemalovic, S.; Britton, C. L., Jr.; Patel, S. V.; Mlsna, T. E.; McCorkle, D.; Warmack, B. Design and Performance of a Microcantilever-Based Hydrogen Sensor. *Sens. Actuators, B* **2003**, *88*, 120−131.
(50) Eriksson, M.; Ekedahl, L. G. Real Time Measurements of Hydrogen Desorption and Absorption During Co Exposures of Pd: Hydrogen Sticking and Dissolution. *Appl. Surf. Sci.* **1998**, *133*, 89−97.
(51) Stuve, E. M.; Jorgensen, S. W.; Madix, R. J. The Adsorption of H_2O on Clean and Oxygen-Covered Pd(100): Formation and Reaction of Oh Groups. *Surf. Sci.* **1984**, *146*, 179−198.

DOI: 10.1021/acsami.9b15111
ACS Appl. Mater. Interfaces 2019, 11, 42349−42357